

CALIS - a CALibration Insertion System for the DarkSide-50 dark matter search experiment

P. Agnes^a, T. Alexander^{ae}, A. Alton^b, K. Arisaka^{ad}, H.O. Back^x,
B. Balding^g, K. Biery^g, G. Bonfini^q, M. Bossaⁱ, A. Brigatti^s, J. Brodsky^x,
F. Budano^y, L. Cadonati^{ae}, F. Calaprice^x, N. Canci^{ad}, A. Candela^q,
H. Cao^x, M. Cariello^h, P. Cavalcante^q, A. Chavarria^d, A. Chepurnov^t,
A.G. Cocco^u, L. Crippa^s, D. D'Angelo^s, M. D'Incecco^q, S. Davini^k,
M. De Deo^q, A. Derbin^v, A. Devoto^c, F. Di Eusonio^x, G. Di Pietro^s,
E. Edkins^j, A. Empl^k, A. Fan^{ad}, G. Fiorillo^u, K. Fomenko^f, G. Forster^{ae},
D. Franco^a, F. Gabriele^q, C. Galbiati^x, A. Goretti^x, L. Grandi^d,
M. Gromov^t, M.Y. Guan^l, Y. Guardincerri^g, B. Hackett^j, K. Herner^g,
E.V. Hungerford^k, Al. Ianni^q, An. Ianni^x, C. Jollet^{aa}, K. Keeter^e,
C. Kendziora^g, S. Kidner^{af,1}, V. Kobylevⁿ, G. Koh^x, D. Korablev^f,
G. Korga^k, A. Kurlej^{ae}, P.X. Li^l, B. Loer^x, P. Lombardi^s, C. Love^{ab},
L. Ludhova^s, S. Luitz^z, Y.Q. Ma^l, I. Machulin^{o,r}, A. Mandaranoⁱ, S. Mari^y,
J. Maricic^j, L. Marini^y, C.J. Martoff^{ab}, A. Meregaglia^{aa}, E. Meroni^s,
P.D. Meyers^{x,*}, R. Milincic^j, D. Montanari^g, A. Monte^{ae}, M. Montuschi^q,
M.E. Monzani^z, P. Mosteiro^x, B. Mount^e, V. Muratova^v, P. Musico^h,
A. Nelson^x, S. Odrowski^q, M. Okounkova^x, M. Orsini^q, F. Ortica^w,
L. Pagani^h, M. Pallavicini^h, E. Pantic^{ad,ac}, L. Papp^{af}, S. Parmeggiano^s,
R. Parsells^x, K. Pelczar^m, N. Pelliccia^w, S. Perasso^a, A. Pocar^{ae},
S. Pordes^g, D. Pugachev^o, H. Qian^x, K. Randle^{ae}, G. Ranucci^s,
A. Razeto^q, B. Reinhold^j, A. Renshaw^{ad}, A. Romani^w, B. Rossi^{x,u},
N. Rossi^q, S.D. Rountree^{af}, D. Sablone^k, P. Saggese^q, R. Saldanha^d,
W. Sands^x, S. Sangiorgio^p, E. Segreto^q, D. Semenov^v, E. Shields^x,
M. Skorokhvatov^{o,r}, O. Smirnov^f, A. Sotnikov^f, C. Stanford^x,
Y. Suvorov^{ad}, R. Tartaglia^q, J. Tatarowicz^{ab}, G. Testera^h, A. Tonazzo^a,
E. Unzhakov^v, R.B. Vogelaar^{af}, M. Wada^x, S. Walker^u, H. Wang^{ad},
Y. Wang^l, A. Watson^{ab}, S. Westerdale^x, M. Wojcik^m, A. Wright^x,
X. Xiang^x, J. Xu^x, C.G. Yang^l, J. Yoo^g, S. Zavatarelli^h, A. Zec^{ae}, C. Zhu^x,
G. Zuzel^{lm}

*Corresponding authors.

Email address: meyers@princeton.edu (P.D. Meyers)

¹Deceased

- ^a*APC, Université Paris Diderot, Sorbonne Paris Cité, Paris 75205, France*
- ^b*Physics and Astronomy Department, Augustana College, Sioux Falls, SD 57197, USA*
- ^c*Physics Department, Università degli Studi and INFN, Cagliari 09042, Italy*
- ^d*Kavli Institute, Enrico Fermi Institute and Dept. of Physics, University of Chicago, Chicago, IL 60637, USA*
- ^e*School of Natural Sciences, Black Hills State University, Spearfish, SD 57799, USA*
- ^f*Joint Institute for Nuclear Research, Dubna 141980, Russia*
- ^g*Fermi National Accelerator Laboratory, Batavia, IL 60510, USA*
- ^h*Physics Department, Università degli Studi and INFN, Genova 16146, Italy*
- ⁱ*Gran Sasso Science Institute, L’Aquila 67100, Italy*
- ^j*Department of Physics and Astronomy, University of Hawai’i, Honolulu, HI 96822, USA*
- ^k*Department of Physics, University of Houston, Houston, TX 77204, USA*
- ^l*Institute of High Energy Physics, Beijing 100049, China*
- ^m*Smoluchowski Institute of Physics, Jagiellonian University, Krakow 30059, Poland*
- ⁿ*Institute for Nuclear Research, National Academy of Sciences of Ukraine, Kiev 03680, Ukraine*
- ^o*National Research Centre Kurchatov Institute, Moscow 123182, Russia*
- ^p*Lawrence Livermore National Laboratory, 7000 East Avenue, Livermore, CA 94550*
- ^q*Laboratori Nazionali del Gran Sasso, Assergi (AQ) 67010, Italy*
- ^r*National Research Nuclear University MEPhI (Moscow Engineering Physics Institute), 115409 Moscow, Russia*
- ^s*Physics Department, Università degli Studi and INFN, Milano 20133, Italy*
- ^t*Skobeltsyn Institute of Nuclear Physics, Lomonosov Moscow State University, Moscow 119991, Russia*
- ^u*Physics Department, Università degli Studi Federico II and INFN, Napoli 80126, Italy*
- ^v*St. Petersburg Nuclear Physics Institute, Gatchina 188350, Russia*
- ^w*Chemistry, Biology and Biotechnology Department, Università degli Studi and INFN, Perugia 06123, Italy*
- ^x*Department of Physics, Princeton University, Princeton, NJ 08544, USA*
- ^y*Physics Department, Università degli Studi Roma Tre and INFN, Roma 00146, Italy*
- ^z*SLAC National Accelerator Laboratory, Menlo Park, CA 94025, USA*
- ^{aa}*IPHC, Université de Strasbourg, CNRS/IN2P3, Strasbourg 67037, France*
- ^{ab}*Physics Department, Temple University, Philadelphia, PA 19122, USA*
- ^{ac}*Physics Department, University of California, Davis, CA 95616, USA*
- ^{ad}*Physics and Astronomy Department, University of California, Los Angeles, CA 90095, USA*
- ^{ae}*Amherst Center for Fundamental Interactions and Physics Department, University of Massachusetts, Amherst, MA 01003, USA*
- ^{af}*Physics Department, Virginia Tech, Blacksburg, VA 24061, USA*

Abstract

In order to calibrate the detector response and detection efficiency of the DarkSide-50 Liquid Argon Time Projection Chamber used for dark

matter detection and the surrounding 30 t organic liquid scintillator neutron veto, we designed, built and implemented a calibration source insertion system (CALIS), which allows to deploy radioactive sources into the liquid scintillator veto. It was commissioned in September 2014 and used successfully in several campaigns to deploy gamma and neutron sources since then.

Keywords:

Dark matter, WIMP, Noble liquid detectors, Low-background detectors, Liquid scintillators, radioactive source calibration

PACS: 95.35.+d, 29.40.Mc, 29.40Gx

¹ **Contents**

² 1	Introduction	3
³ 2	Design Requirements & Hardware Implementation	4
⁴ 2.1	Purpose	4
⁵ 2.2	Deployment & Articulation Mechanism	6
⁶ 2.3	Housing & Scintillator	9
⁷ 2.4	Design Requirements	9
⁸ 2.5	Hardware Details	11
⁹ 2.6	Degrees of freedom of the system	15
¹⁰ 3	Testing, Cleaning and Commissioning	17
¹¹ 3.1	Operational Procedure	19
¹² 4	Calibration Campaigns	21
¹³ 4.1	Radioactive Sources	21
¹⁴ 4.2	Timeline of the Calibration Campaigns and Stability	21
¹⁵ 4.3	TPC Calibration	24
¹⁶ 4.4	Liquid Scintillator Veto	25
¹⁷ 5	Conclusions	26

¹⁸ **1. Introduction**

¹⁹ DarkSide-50 is a Liquid Argon Time Projection Chamber (LAr TPC),
²⁰ operated in the Gran Sasso National Laboratory (LNGS) in Italy to search

21 for nuclear recoils induced by weakly interacting massive particles (WIMPs).
22 A first physics result was reported in [?] based on 50 live days of data col-
23 lected with Atmospheric Argon (AAr), providing the most sensitive limit
24 on a dark matter search using a LAr TPC to date with a 90% CL upper
25 limit on the WIMP-nucleon spin-independent cross section of 6.1×10^{-44}
26 cm^2 for a WIMP mass of 100 GeV/c².

27 The DarkSide-50 apparatus has been described in detail in [?], but
28 for the reader's convenience a short reminder is given. As shown in
29 fig. 1 it features a LAr TPC surrounded by a 30 t liquid scintillator-based
30 veto (LSV) system, which in turn is housed in a water Cerenkov detector
31 (WCD), both of which help to measure in-situ and suppress radiogenic
32 and cosmogenic backgrounds. On top of the WCD there is a radon-free
33 clean room (CRH) which houses the cryogenic supply system, the elec-
34 tronics and slow control software, among other things (Fig. 2). The inside
35 of the LSV is accessible from CRH through four access ports nick named
36 organ pipes, which end at their top in gate valves.

37 2. Design Requirements & Hardware Implementation

38 2.1. Purpose

39 Electronics gain calibration of the WCD, LSV and TPC is done with
40 dedicated Laser systems, that are in place in each of the three subdetec-
41 tors. The Laser calibration in the WCD is sufficient to veto muons (and
42 their secondaries) with high efficiency [?]. The TPC detector response
43 has been calibrated using the internal 39Ar as well as 83mKr, that has
44 been added into the LAr recirculation system during dedicated calibra-
45 tion campaigns [?].

46 The goal with the CALibration source Insertion System (CALIS) is to
47 study and calibrate the detector response of the TPC and the LSV as well
48 as the detection efficiency of internal neutrons interacting in the TPC and
49 LSV using radioactive gamma and neutron sources. This complements
50 and extends the physics reach of internal source and Laser calibration.

51 The center of the LSV is about 6 m below the gate valve inside CRH
52 and the 6" wide organ pipes are vertical, yet about 80 cm off center in the
53 XY plane as shown in Fig. 2. For TPC calibration the radioactive source
54 has to be positioned in immediate contact with the cryostat, in order
55 to minimize rate losses through absorption in particular for low energy
56 sources such as ⁵⁷Co (122 keV).

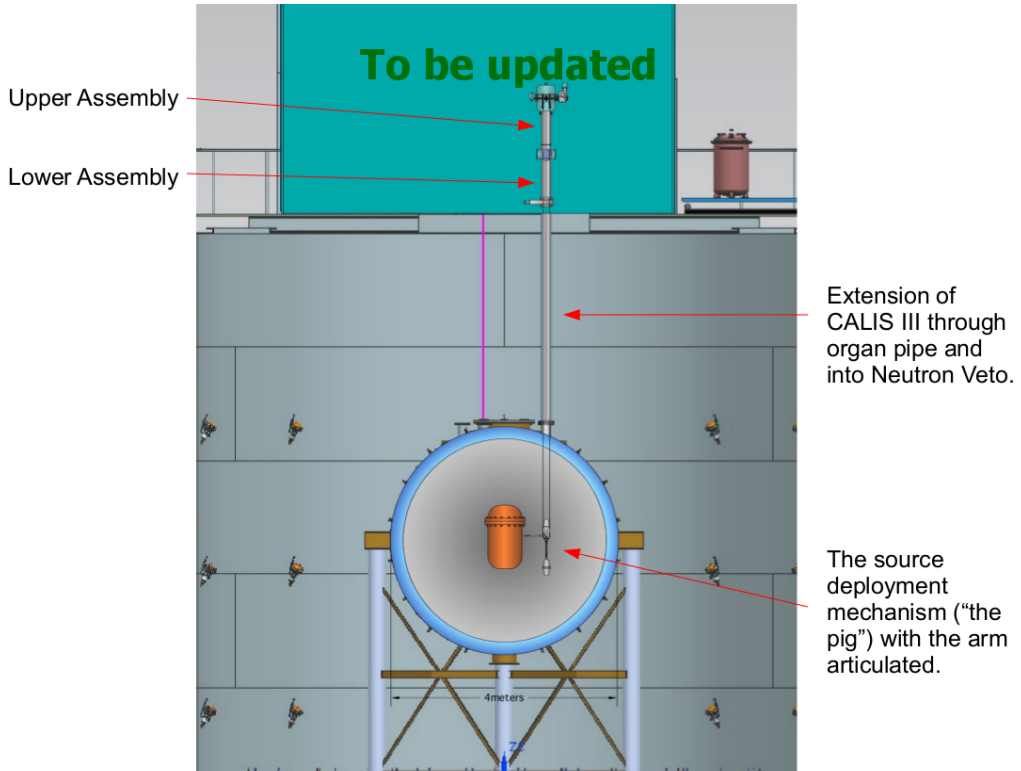


Figure 1: A conceptual drawing of CALIS installed in the radon-suppressed clean room CRH atop the water Cerenkov detector (WCD) and with the deployment device containing the source deployed in the liquid scintillator veto (LSV) next to the liquid argon time projection chamber's (LAr TPC) cryostat. The clean room and the LSV are connected through four access ports nick named organ pipes (only one of which is drawn in the sketch above: (1)). All four organ pipes end in CRH at gate valves (2) which can be manually opened or closed. During normal operations all four organ pipes are closed. Not included in the sketch are tubes connecting the cryogenic systems in CRH to the cryostat in the LSV ((3) and (4)).

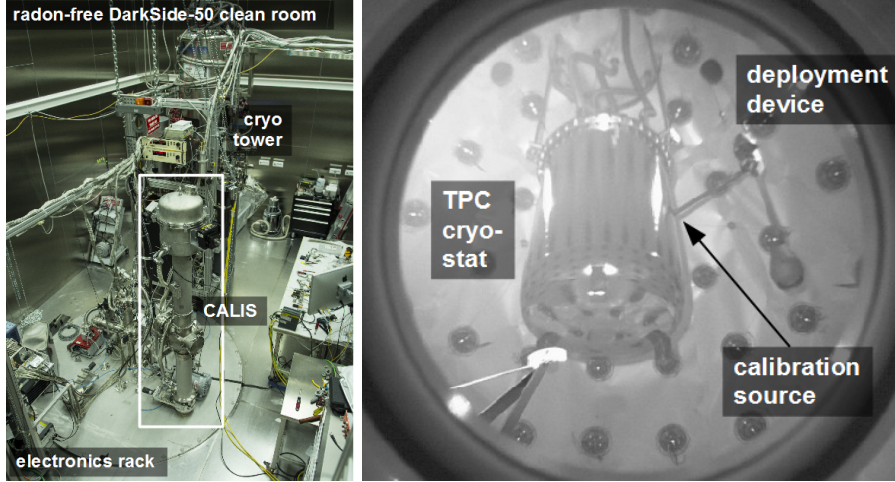


Figure 2: *left*: CALIS after installation inside the CRH room. The organ pipe is 80 cm off-center wrt. the TPC center in the horizontal XY plane. *right*: Photograph taken with a camera looking upwards into the LSV from the bottom. It shows the source deployment device deployed through one of the organ pipes visible on the top right. The arm is articulated and the source is next to the cryostat of the LAr TPC.

57 2.2. Deployment & Articulation Mechanism

58 This requirement precludes a single cable solution deployed from
 59 within a glove box as has been used in several scintillator experiments
 60 [? ?]. Instead the apparatus consists of the housing, which has been
 61 installed in CRH (Fig. 2, left) and the deployment device is attached to
 62 the housing through two stainless steel cables that are wound up on cable
 63 spools and allow the lowering of the device into the LSV, next to the
 64 cryostat (Fig. 2, right).

65 The stepper motor moves both cable spools concurrently and sends
 66 the deployment device into the LSV. An absolute encoder monitors its
 67 current position, even in the absence of power. The stepper motor is
 68 controlled via a simple graphical LabVIEW interface, run on a dedicated
 69 laptop, in which the current z-position is shown and a target z-position
 70 can be provided by the operator. Z-positions are given in motor step
 71 counts, an arbitrary unit which has been calibrated outside CRH in meters
 72 (Fig. 4) and relative to the TPC using the t-drift distribution of calibration
 73 data (Fig. 15, p. 26).

74 Articulation of the arm is done manually via the articulation wheel.
 75 This affects only the cable spool close to the articulation wheel, the left

in fig.3 the drawing should show the arm articulate towards the left, since when the left spool is engaged, the arm articulates towards the left.

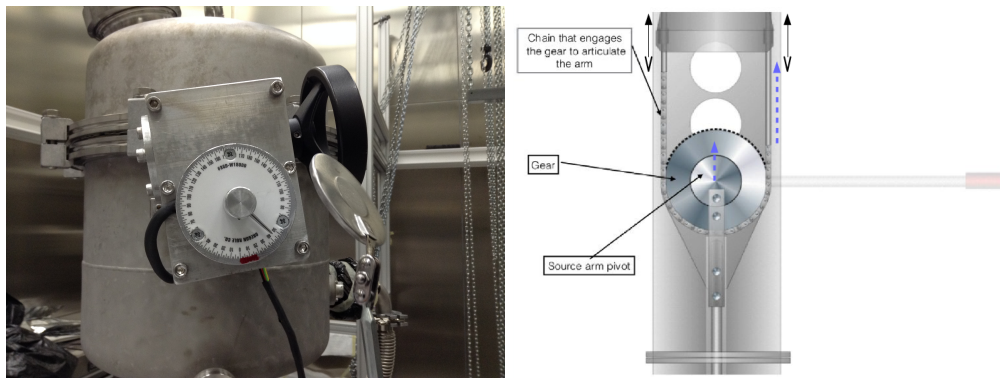
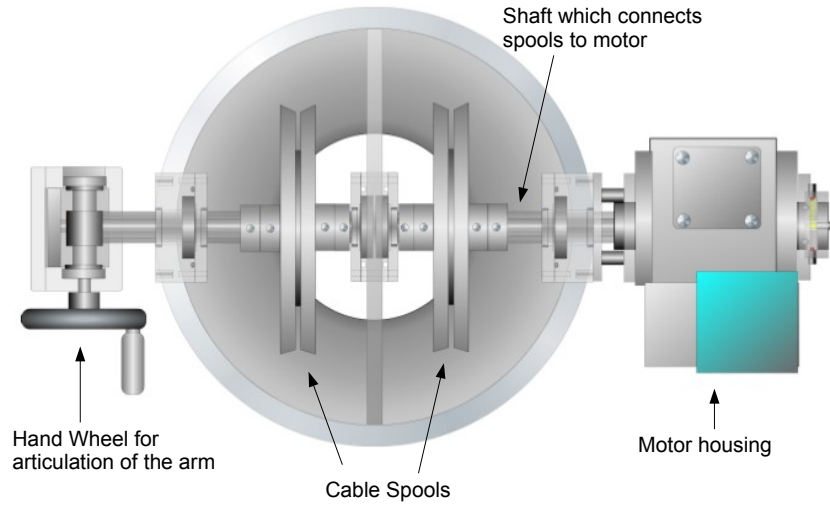


Figure 3: *top*: Inside view of the drive mechanism's components seen from the top of CALIS. The stepper motor inside the motor housing drives both cable spools concurrently, thereby lowering the calibration device into the LSV. An absolute encoder provides the current position of the deployment device. The hand wheel on the left is connected to the left spool only (*bottom left*). When engaged, it drives the gear to transfer the rotation of the articulation wheel into a rotation of the source arm (*bottom right*). The chain has a guard rail, not shown in the drawing, that ensures that the chain can never come off the gear.

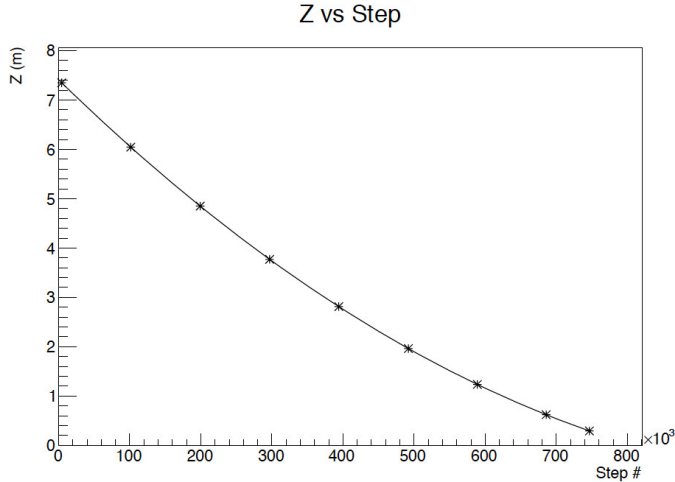


Figure 4: Plot of the z position of the deployment device versus the step position of the motor. The non-linear correspondence between the number of steps and the length of cable deployed arises as follows: As the cable winds around the spool, the winding radius changes, increasing as the pig is lifted and decreasing as it is lowered. A motor step count corresponds to a fixed angular distance $d\theta$, yet the amount of cable deployed during this motor step count is $\text{winding radius} \cdot d\theta$. As the winding radius changes as a function of z position, the fraction of deployed cable per motor step count changes.

76 one in Fig. 3, thereby shortening the left cable wrt. to the right cable
 77 and engaging the gear through a chain (Fig. 3). As a result the arm is
 78 articulated and the pivot center is lifted. The non-linearity arising from
 79 the change in winding radius on the cable spools affects also the amount
 80 of rotation required by the hand wheel for horizontal articulation of the
 81 source arm. The degrees corresponding to a horizontal articulation has
 82 been calibrated as a function of cable length deployed prior to installation
 83 in CRH.

84 Articulation and a movement in z -direction are mutually exclusive
 85 since the articulation of the arm leads to more wound up cable on the
 86 spool close to the articulation wheel wrt. the other. If then in deploy-
 87 ment mode both spools would be rotated simultaneously with the same
 88 angular speed, the cable close to the articulation wheel would wind up
 89 faster than the other, which would lead to a build up of difference in cable
 90 length and the deployment device would only be hanging on one cable.
 91 In order to avoid an imbalanced z -movement the arm has to be dearticu-
 92 lated fully before a change in z -position can be initiated. This is enforced
 93 by an electric switch preventing z -movement, which is disengaged only

⁹⁴ when the arm is fully dearticulated.

⁹⁵ 2.3. *Housing & Scintillator*

⁹⁶ Besides providing mechanical support for the deployment device via
⁹⁷ the cable spools, the housing is the important interface between CRH and
⁹⁸ the LSV, through which sources are exchanged, while protecting the liq-
⁹⁹ uid scintillator and avoiding human contact with even traces of liquid
¹⁰⁰ scintillator vapor. It plays the same role as a glove box for other cali-
¹⁰¹ bration systems with a narrower foot print. The liquid scintillator is a
¹⁰² mixture of PC and TMB² with the wavelength shifter PPO[?]. It may not
¹⁰³ get exposed to oxygen or water as is present in normal clean room air
¹⁰⁴ and also contamination with ²²²Rn and its long-lived radioactive daugh-
¹⁰⁵ ter molecules has to be avoided.

¹⁰⁶ Vacuum and nitrogen pressurization systems have been developed ??.
¹⁰⁷ On the other hand TMB vapors and residues could form ...

¹⁰⁸ *ToDo: more precise on risks of contact of TMB with air/ water. What are the*
¹⁰⁹ *dangers compared to a PC only scintillator?*

¹¹⁰ 2.4. *Design Requirements*

¹¹¹ The design of CALIS is shaped by the following requirements, thereby
¹¹² following the design principle of “form follows function”:

- ¹¹³ • to allow source exchanges and safely deploy them at various posi-
¹¹⁴ tions inside the LSV,
- ¹¹⁵ • protecting the scintillator from oxygen and water at any time, in
¹¹⁶ particular during deployments and being able to articulate a source
¹¹⁷ arm in order to bring the source next to the cryostat. Also pro-
¹¹⁸ tection and safety mechanisms that avoid exposure of personal to
¹¹⁹ scintillators are in place.
- ¹²⁰ • To complement studies of nuclear recoils with neutron sources (²⁴¹Am⁹Be
¹²¹ and ²⁴¹Am¹³C), it is planned to deploy a neutron gun inside a dedi-
¹²² cated deployment device currently under development (Section ??).

²The concentration of TMB has varied during campaigns (see Sec. 4).

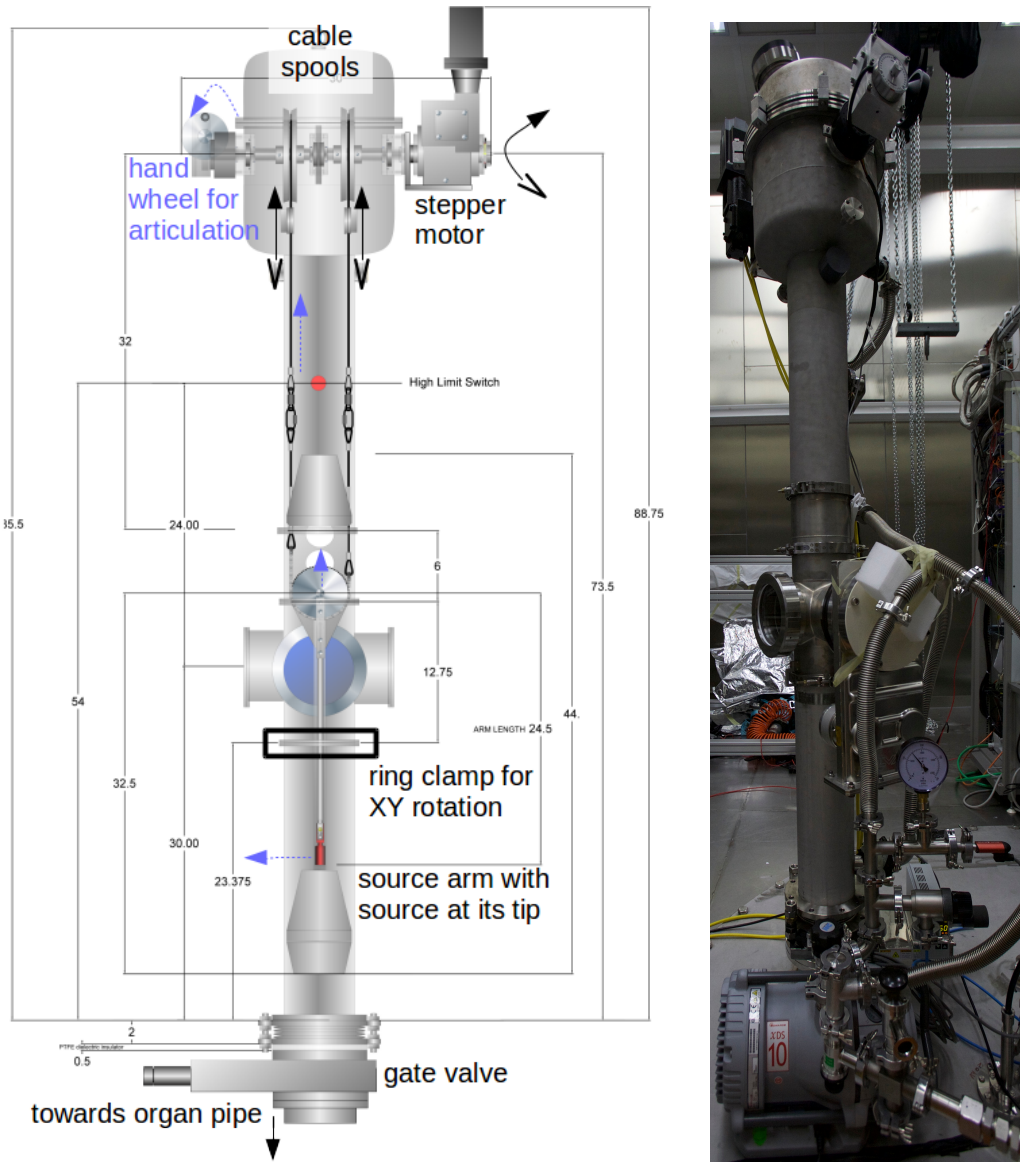


Figure 5: Mechanical drawing of CALIS showing the housing and the deployment device. Dimensions are in inches. (The total height of 88.75 inches corresponds to 225.425 cm.) The two modes of operation are illustrated: In order to move the deployment device down into the LSV or back up the stepper motor moves both cable spools simultaneously. In order to articulate, the articulation wheel is rotated manually, which affects only the left spool, thereby shortening the left cable wrt. to the right cable thereby articulating the arm and lifting the pivot center. The amount of lifting and the amount of rotations until a horizontal articulation is reached has been calibrated prior to installation in CRH (Sec. ??)

- 123 • All materials that come in contact with the scintillator veto are made
 124 of stainless steel and teflon except for the sealing o-rings which are
 125 made out of viton. All three materials (stainless steel, teflon, and
 126 viton) are certified materials for contact with TMB and PC.
- 127 • Before assembly in CRH, each component of CALIS, the ones intro-
 128 duced into the scintillator as well as those in the clean room CRH,
 129 have been subjected to the official cleaning procedure [?].

130 This results in further hardware design choices and requirements that
 131 are discussed below.

132 2.5. Hardware Details

133 2.5.1. Housing

134 Here the design of the housing shown in fig. 5 is described in more
 135 detail. Starting at the gate valve inside the clean room CRH on which
 136 CALIS has been installed, a a teflon disk allows to electrically isolate
 137 CALIS from ground, even though during normal operations the CALIS
 138 housing is also connected to ground. A tripod with a bellow has been
 139 used to vertically align the housing right after installation on the gate
 140 valve. The bellow is connected to a 23.375" long cylindrical stainless steel
 141 enclosure pipe. It has the same diameter as the organ pipe (6") and leads
 142 into a view port (depicted in blue in fig. 5) and which is the access point
 143 for accessing the source arm and exchanging sources.

144 Above the view port is the upper assembly, which is a stainless steel
 145 cylindrical enclosure that houses the cable drive mechanism, including
 146 the cable spools the stepper motor and the articulation mechanism, al-
 147 ready described in Sec. 2.2.

148 CALIS offers various safety features to ensure that the device runs
 149 smoothly, no components are lost inside the detector, avoid any contam-
 150 ination of the detector by dirty or incompatible materials, maintain pres-
 151 sure and avoid introduction of oxygen or water in contact with the LS
 152 and TMB, operation in the volume that excludes possibility of contact
 153 with PMTs or light pulsers (pacman) attached to each PMT.

154 2.5.2. Safety features

155 **Drive mechanism:** The drive mechanism is a stepper motor that has an
 156 integrated absolute encoder providing the location of the source at

Is there
any public
document on
the cleaning
procedures?
Is this
necessary to
quote?

157 all times, even in the event of a power failure. In the event of a
158 power failure, the magnetic break ensures there is no movement
159 of the pig. The torque of the servo motor is limited in case of an
160 unexpected load.

161 The speed reducer (gears) is a double worm gear design. The pri-
162 mary worm gear has a 50:1 reduction and the secondary worm has
163 a 82:1 reduction. The input speed of the servo motor is 2400 RPMs
164 and the output is 0.6 RPM and has the weight capacity of 148 lbs. In
165 the event of a power failure the speed reducer has the ability to hold
166 the load at any position without back drive. The speed of the motor
167 has been limited to 0.4 cm/s which minimizes any lateral oscillation
168 of the pig during lowering and raising the source. Additionally, this
169 is the maximum speed at which the motor is not overheating.

170 **Manual retraction system:** In the unlikely case of a complete motor fail-
171 ure while the source is deployed, it is possible to manually retract
172 the pig back to its home position and close the gate valve. The mo-
173 tor is disengaged, and wrench is used to manually wind the cable
174 back onthe spools and retract the pig back above the gate valve.

175 **Cable strength and length:** The cables holding the pig have been rated
176 for loads over 590 kg, while the weight of the pig is at the level of
177 10-15 kg so well below the breaking strength of the cable. The cable
178 length has been established so that the maximum depth at which the
179 pig can be deployed is above the level of the PMTs inside the LSV.
180 In case, the command is given to deploy to greater depth, the cable
181 completely unwinds and then rewinds in the opposite direction,
182 which then effectively retracts the pig to a higher z-position until
183 the preset motor count of steps is reached.

184 **Upper limit switch:** The motor has an absolute encoder and step posi-
185 tion is never lost even in the case when the motor loses power. When
186 the pig has reached its home position within the upper assembly it
187 will stop. However, if the top of the pig continues past its home
188 position (based on the number of steps given), it will not be able to
189 pass its home position thanks to the upper limit switch that will be
190 triggered in that case.

191 Neither the manual retraction system has been used nor has the
192 upper limit switch been activated during calibration campaigns.

193 **Light and leak tightness of CALIS:** When the deployment device is next
194 to the cryostat the gate valve is open and we take also data with the
195 LSV. A prerequisite is that the housing is absolute light tight and
196 pressure leak tight. All view ports have light tight covers for when
197 the organ pipe gate valve is open. Both light and leak tightness has
198 been extensively validated throughout the manufacturing process
199 until including commissioning (Sec. 3).

200 **Maximum deployment depth keeps the deployment device out of reach of the bottom PMT**

201

202 *2.5.3. Deployment device*

203 The pig (Fig. ??) contains the support structure for the arm which
204 holds the source at its end. This piece is equipped with tapered cones on
205 the top and bottom that ensure that the ends do not get snagged on inner
206 edges of the organ pipe as it is moving up and down. It is attached to
207 the housing by two cables. Swivel hooks are employed in the attachment
208 of the cables to the pig that allow the cables to move freely and not get
209 tangled. There are two weights built into the device, one cylindrical in the
210 conical cap above the rotation gear mechanism and one inside the cones
211 at the bottom end of the device. Both help to minimize any lateral motion
212 or oscillations during deployment and articulation and dearticulation es-
213 pecially. It also ensures smooth motion of the deployment device into the
214 organ pipe and back to the home position inside the housing.

215 *2.5.4. Source holder and arms*

216 A source arm and the source holder are attached to the articulation
217 gear (Fig. 6). Different arm lengths have been prepared with a maximum
218 arm length of 62 cm, the arm length thereby being measured from the
219 pivot point of the rotation gear to the tip of the source holder. This arm
220 length allows the source to be placed in immediate contact with the cryo-
221 stat (Fig. 2, right), as the center axis of the organ pipe is 81 cm from the
222 TPC center and the cryostat has an outer radius of 32 cm. The 62 cm
223 arm was used for most of the deployments in the past calibration cam-
224 paigns (Sec. ??). Inside the source holder the radioactive source is placed,

225 pressed to the tip and held in place via a spring during deployment, ar-
226 tication and dearticulation. The source holder is sealed such that no
227 liquid scintillator can enter during the deployment. This has also been
228 verified during each source extraction, that no liquid was found on the
229 inside.



Figure 6: Source holder that connects to an arm and to the articulation gear of the deployment device. The source, here a ^{133}Ba source is pressed to the tip of the source holder via a spring.

230 *2.5.5. Securing of the source*

231 All connection points for the source and arm have been secured with
232 two push locking pins that cannot be disengaged without a person press-
233 ing the pin. The source holder is held in place via a locking mechanism
234 and two locking pins. When the source is attached to the arm, the source
235 container must be slid over a protruding pin. There is a sliding locking
236 mechanism that interlocks onto the pin. Once the source is locked into
237 position there are 2 additional locking pins that are put into place (one
238 above and one below the source holder pin), each of which have a button
239 that must be depressed in order for the pins to be released. In addition,
240 the source holder and the 2 locking pins will all be tethered from outside
241 the view port until they are locked in place eliminating the possibility
242 of accidental falling. The tethering will happen before installation of the
243 source and before the removal of the source. The cables used to tether the
244 pins and the source holder during installation and removal will be de-
245 tached after installation and prior to deployment to avoid the possibility
246 of the arm getting entangled.

247 2.6. Degrees of freedom of the system

248 CALIS has the capability to deploy sources at various positions inside
 249 the LSV. Besides the movement along z up to the maximum cable length,
 250 there is the possibility to articulate at an angle of θ between 90° and 180° ,
 251 where θ is the zenith-angle (Fig. 7). Degrees between 0° and 90° are
 252 excluded because the end of the articulation chain is reached at an angle
 253 of 90° (see Fig. 3).

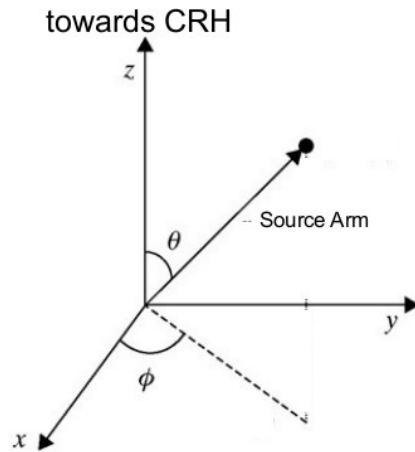


Figure 7: Spherical coordinate system used for establishing the direction of the rotation of CALIS-III and the articulation of the source arm. θ is kept at 90° when arm is articulated, and at 180° when dearticulated. x-axis is the direction toward the center of the detector.

254 2.6.1. Rotation in the XY plane

255 Below the view port is a sealed connection that has an o-ring seal
 256 and uses a ring clamp to compress the seal. The clamp can be slightly
 257 loosened to allow the assembly above and including the view port to be
 258 rotated with respect to the lower assembly and the detector. This rotation
 259 in the XY plane can even be performed while the gate valve is opened
 260 and the deployment device is deployed next to the cryostat, since the seal
 261 is helium leak and light tight even when loosened.

262 In principle a rotation in 360° can be done, except when the arm
 263 would interfere with the cryostat. This has been used in one of the cali-
 264 bration campaigns to deploy a neutron source directly next to the cryostat
 265 and rotated away by 90° in order to study optical shadowing effects from
 266 the cryostat (Sec. 4).

My impression is that a drawing to scale with the cryostat, the TPCthe organ pipe and the source arm would be good here

267 For articulation, there is currently a choice of three arm lengths—
268 40.31 cm, 57.15 cm and 62 cm.

269 Each of these lengths are measured from the center line of the organ
270 pipe to the end of the source holder. The arm lengths, 57.15 cm and 62 cm
271 are intentionally made too long as they will be used to determine the
272 exact location of the cryostat; some uncertainty in the cryostat's z and
273 lateral position exist at the level of 3 - 4 cm. The organ pipe we intend
274 to use is 81 cm distant from the cryostat center (and the geometric center
275 of the LSV sphere) as measured from the center line of the organ pipe.
276 The cryostat is 32 cm in radius, which leaves a distance of ~49 cm to be
277 reached by the arm.

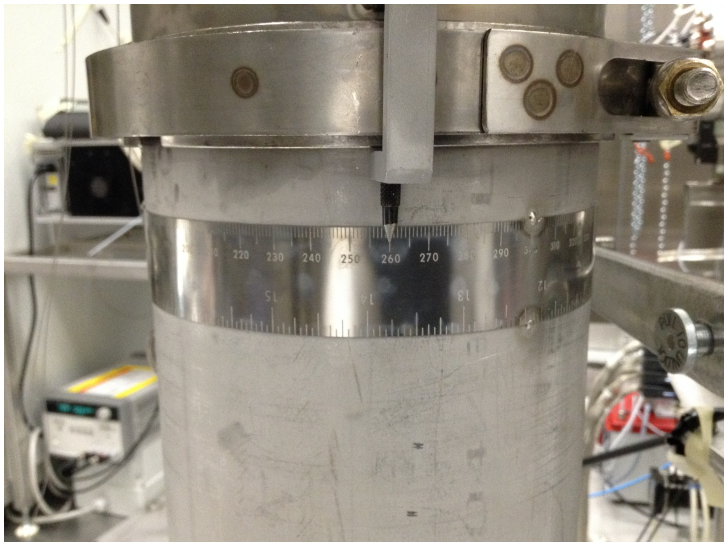


Figure 8: Ring clamp with the angle measuring strip shown below. In order to perform azimuthal rotation, the ring clamp is slightly loosened, and the entire upper assembly is rotated with respect to the lower assembly, along with the deployment device. The angle of rotation is read out from the strip that goes around the pipe. The strip is in mm, which has then been calibrated in degrees.

278 2.6.2. “No fly” zone

279 Right above the cryostat where there are many supply tubes for the
280 TPC a “no fly” zone has been defined. In this region no part of the
281 deployment device may enter, in particular not the source arm.

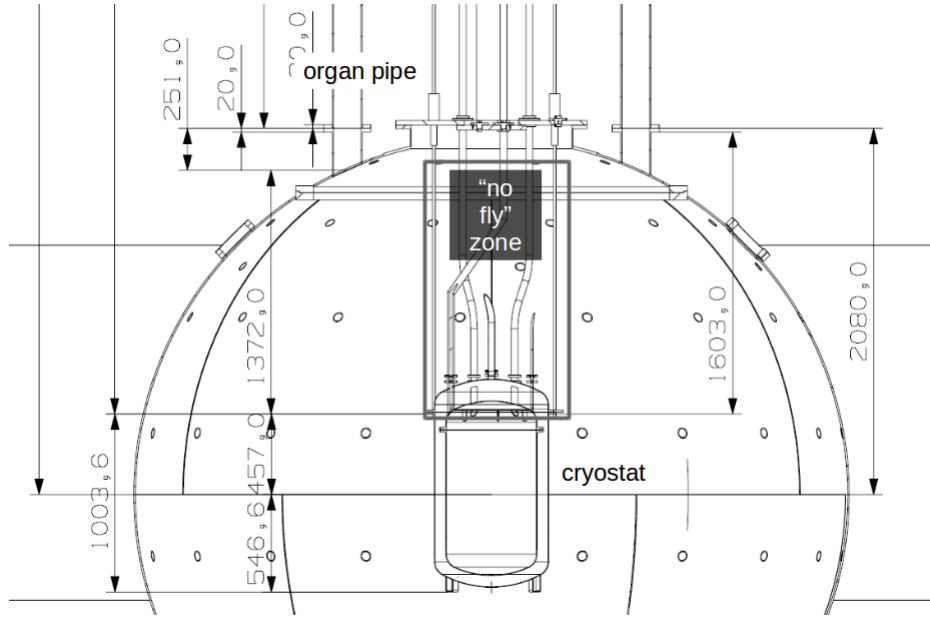


Figure 9: "No fly" zone for the CALIS source arm.

282 2.6.3. *Default configuration*

283 By default the deployment device has been deployed with the longest
 284 arm (62 cm), at the center of the active volume of the TPC, with the arm
 285 rotated in the XY plane until contact with the cryostat has been made.
 286 Further details are provided in Sec. 4.

287 Other degrees of freedom could involve shorter arm lengths, while
 288 longer arm lengths have been discussed but would require hardware
 289 modifications to the deployment device. Out of a total of four organ
 290 pipes a second one would be available for source calibration. A change
 291 in organ pipe would require a bigger effort involving also the crane in
 292 order to dismount CALIS and reinstall it on the other organ pipe. The
 293 remaining two pipes are too close to the cryo tower or reserved for the
 294 SABRE experiment [?].

295 Finally CALIS is designed to house also a different deployment device,
 296 such as currently being planned for the neutron gun [?].

297 **3. Testing, Cleaning and Commissioning**

298 Staged approach in testing: FNALL basic functionality test LNGS:
 299 Shipment of CALIS sub-assembled to LNGS

300 approval for installation cleaning according to official cleaning proce-
301 dures and installation on the gate valve of CRH

302 after installation: commissioning functional tests, etc.
303 testing site that allowed full deployment of CALIS

304 Testing of CALIS has been performed at FNAL in the second half
305 of August and first half of September 2014. CALIS was installed in a
306 building with the high bay, on a high platform, so that the full length
307 deployment tests could be performed. The tests are repeated at LNGS
308 prior to cleaning the system, and some validation tests are foreseen at the
309 time of installation in CRH. Several different tests have been conducted:

310 • Test for light and helium leak tightness of the whole system
311 • Validation of motor controls and LabView based graphical user in-
312 terface

313 • Validation of functionality of the safety features (upper limit and
314 arm retraction switch)

315 • Accuracy and precision in source position: tests with and without
316 source arm articulation

317 • calibration of the motor step counts in meters with and without
318 articulation and t-drift +

319 • scenarios: before and after power failure

320 • test nitrogen and vacuum systems: Measure the amount of time to
321 evacuate the device and purge with nitrogen (how long does it take
322 in reality?)

323 • 1 cm uncertainty

324 • At LNGS the XY and Z position of the source was fully character-
325 ized and calibrated in meters.

326 A more detailed description of tests performed at FNAL and LNGS
327 can be found in [? ?].

328 Tests in air and in the LSV's scintillator revealed that the source po-
329 sition accuracy is dominated by uncertainties during articulation. The
330 positioning in z before articulation is highly accurate and precise: The

*This sentence
might require
some more
qualifi-
cation...
Too much
advertising.*

331 deployment speed is very low, barely visible ot the naked eye (mm/s),
332 which minimizes the lateral motion during deployment and contact with
333 housing or organ pipe is avoided during deployment. Yet during ar-
334 tication an uncertainty in the XY position is arising from tiny laterally
335 imbalanced forces resulting from the pull on the articulating cable. To en-
336 sure deployment precision we worked out a procedure to make reliably
337 gentle contact: after positioning the deployment device in z, articulate
338 to horizontal while the source arm is pointing away from the cryostat,
339 finally bring the source into contact with the cryostat through a rotation
340 in XY while monitoring the PMT scaler rates, which increase while the
341 source is approaching, yet stalls as soon as contact with the cryostat is
342 made, even if the rotation in XY continues.

343 *3.1. Operational Procedure*

344 After the testing and commissioning CALIS has been installed inside
345 CRH...

346 Well, there also have been test deployments before that.

347 *3.1.1. Source Insertion*

348 *3.1.2. 3 special positions*

349 home position or parking position - gate valve closed. The
350 center of the TPC.

351 Full extension position - length of the cable.

352 *3.1.3. Vacuum evacuation (flushing) and nitrogen purging*

353 One of the most important features of this system is making sure that
354 the TMB and PC residue on the device are extracted from CALIS III prior
355 to opening access ports to exchnage source or arms. This is important for
356 safe working level of the people involved and for the detector. This can be
357 addressed through a system evacuation and nitrogen purge. To accelerate
358 the removal of the TMB in the scintillator fluid residue that is left after a
359 deployment, CALIS III will undergo an evacuation with a vacuum pump.
360 By lowering the pressure inside of CALIS below the vapor pressure of
361 the TMB, it will cause the TMB to outgas and be removed through the
362 vent line of the vacuum pump. An additional step to remove the TMB
363 is to purge using N₂. We will need to limit the potential flow rate of the
364 nitrogen to ensure that an ODH (Oxygen Deficiency Hazard) condition

365 is avoided in CRH. Only once this is accomplished, will the view port be
366 allowed to be opened and the source handled.

367 The entire CALIS III has been tested at FNAL to hold pressure. The
368 system will be tested again after installation on the gate valve.

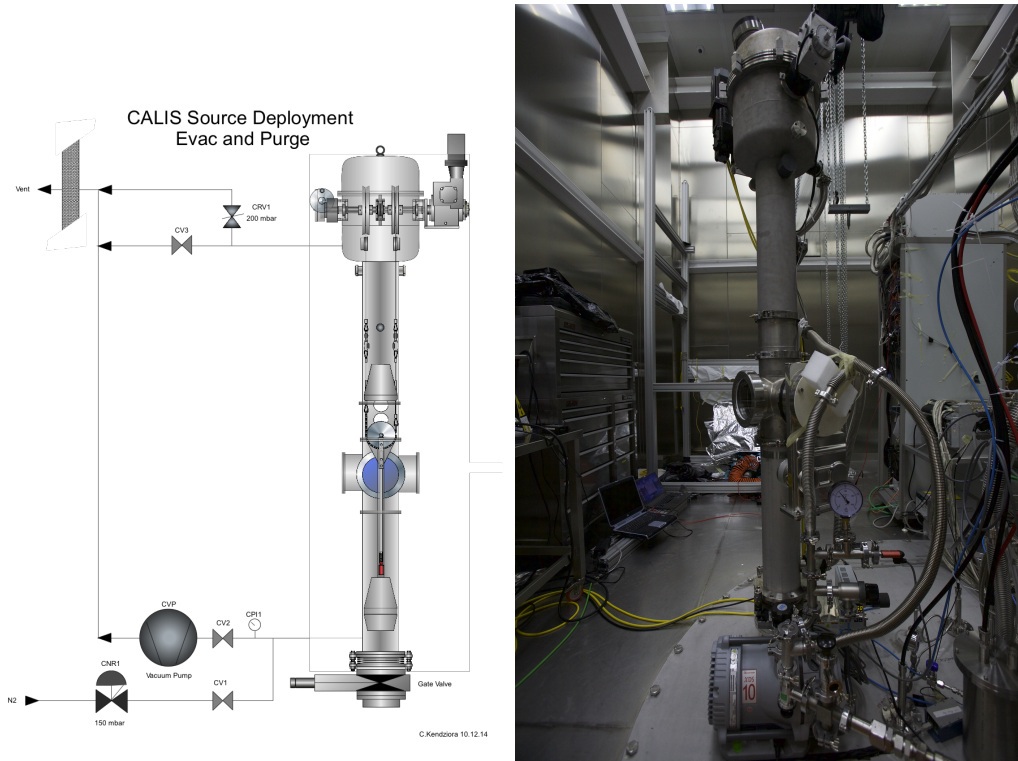


Figure 10: flushing and nitrogen purging system.

369 *Opening the Gate Valve.*

370 *3.1.4. Positioning of Source*
371 *Contact with Cryostat.*

372 *Cameras.*

373 *3.1.5. Source Retraction and Extraction*

374 The source may not get in contact with the liquid scintillator. It is
375 therefore sealed during the deployment in a dedicated source holder. In
376 order to exchange sources the source arm and source holder has to be

377 extracted from the pig into CRH and thereby comes in contact with nor-
378 mal air, containing oxygen and traces of water. After insertion a flush &
379 purge cycle is used to reduce, as known from glove boxes. No glove box
380 present. Much more compact design.

381 After each deployment check that there is no leakage of Scintillator
382 inside the source holder.

383 for what is helium leak tightness necessary? What was tested for
384 helium leak tightness.

385 4. Calibration Campaigns

386 4.1. Radioactive Sources

387 For the calibration of the LSV detector response and the TPC's re-
388 sponse to electron recoils (ER) we selected ^{57}Co , ^{133}Ba and ^{137}Cs . In a
389 later calibration campaign also ^{22}Na has been deployed. They allow a
390 cross-calibration with ^{83m}Kr , that has been injected in the Ar recirculation
391 system during dedicated campaigns and the internal ^{39}Ar , as they cover
392 the energy range of ^{39}Ar (see also Table 1 and Fig. 11).

393 After a preselection of gamma source energies, detailed studies with
394 the DarkSide Monte Carlo G4DS [?] were performed to select appropri-
395 ate source activities and check the feasibility and physics reach of various
396 deployment positions. Considering also constraints from the LSV and
397 TPC DAQs, sources with suitable activities were identified for deploy-
398 ment (Table 1).

399 Energy variables are calibrated in photo-electrons (PE) using dedi-
400 cated Laser calibration runs, in which the single PE charge spectra for
401 each PMT are fitted and a PE-charge gain is determined. These Laser
402 runs are also an integral part of a calibration campaign requiring a Laser
403 run at least on each change in DAQ or CALIS configuration, such as drift
404 field changes or source position changes.

possible upgrade for fig.16: all measured spectra overlayed at a fixed HV: 83mKr, Co57, Ba133, Cs137 (either null field or 200 V/cm) - ask Brianne? Also for her thesis?

get the numbers for Na22 in the table

405 4.2. Timeline of the Calibration Campaigns and Stability

406 Between October 2014 and April 2016 the following calibration cam-
407 paigns have been performed:

- 408 • The first extensive campaign involving all gamma sources and both
409 the high and low activity AmBe neutron source took place in Oc-
410 tober and November 2014 at LNGS. The TPC was filled with atmo-
411 spheric argon with an inherent trigger rate of approx. 50 Hz from

has LNGS been introduced?

has atmospheric argon been introduced and underground argon?

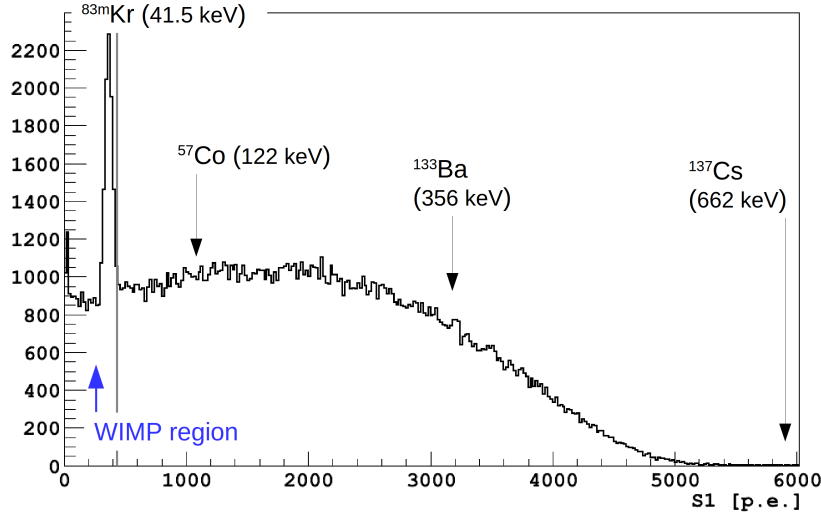


Figure 11: Scintillation spectrum (S1) at null field showing a ^{83m}Kr peak on the ^{39}Ar β spectrum. The energies of the three gamma sources are indicated and cover the full range of the ^{39}Ar spectrum.

Table 1: Gamma sources deployed in DS-50, ^{39}Ar and ^{83m}Kr [29]. Interaction length is in LAr. Activity of ^{39}Ar has been approx. 50 Hz during AAr filling and negligible in the UAr phase. The Kr source activity varied from campaign to campaign, but was in the range of a few kBq to some tens of kBq.

source	type	energy	half life	interact. length	activity
^{57}Co	γ	122 keV	0.744 y	4.4 cm	35 kBq
^{133}Ba	γ	356 keV	10.54 y	7.5 cm	2 kBq
^{137}Cs	γ	662 keV	30.2 y	9.5 cm	0.65 kBq
^{22}Na	γ	2 · 511 keV + 1274 keV	xxx y	xxx cm	11 kBq
^{39}Ar	β	565 keV endpoint	xxx y	sub-mm	50 Hz
^{83m}Kr	2 β	32.1 keV + 9.1 keV	xxx y	sub-mm	

³⁹Ar. The liquid scintillator of the LSV contained a PC only scintillator with < 0.1% TMB and 1.4 g/l PPO as wavelength shifter.

- In January and February 2015 a second campaign focusing on the LSV calibration using the low activity AmBe source was performed. Prior to that the LSV has been reconstituted with 5 % TMB. Two deployments were performed at two different PPO concentrations (0.7 g/l and 1.4 g/l), allowing to study the impact of the PPO concentration on alpha and gamma quenching. (1.4 g/l is our nominal PPO concentration, see also Fig. 16, right)
 - In August 2015 a ^{22}Na source has been deployed next to the cryostat for TPC calibration. This was the first gamma source calibration campaign after the UAr deployment within DarkSide-50.
 - In December 2015 an $^{241}\text{Am}^{13}\text{C}$ neutron source has been deployed, allowing an in-depth study of the detection efficiency of the prompt neutron recoil signal in the absence of the correlated 4.4 MeV gamma, obfuscating the neutron recoil signal in case of an AmBe source.

As shown in Fig. 12 the calibration campaigns have not affected negatively the light yield or introduced radioactivity into the LSV.

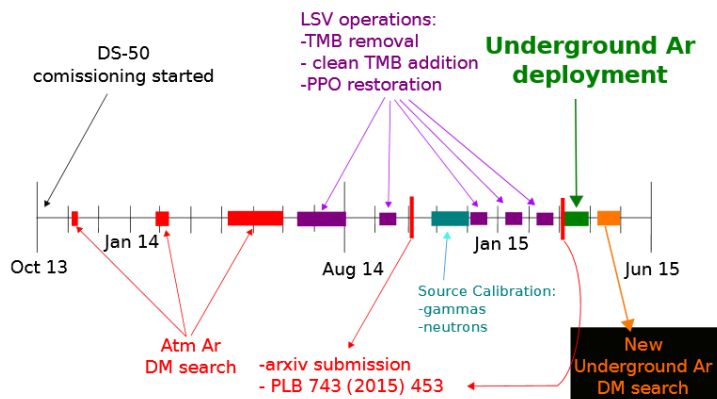


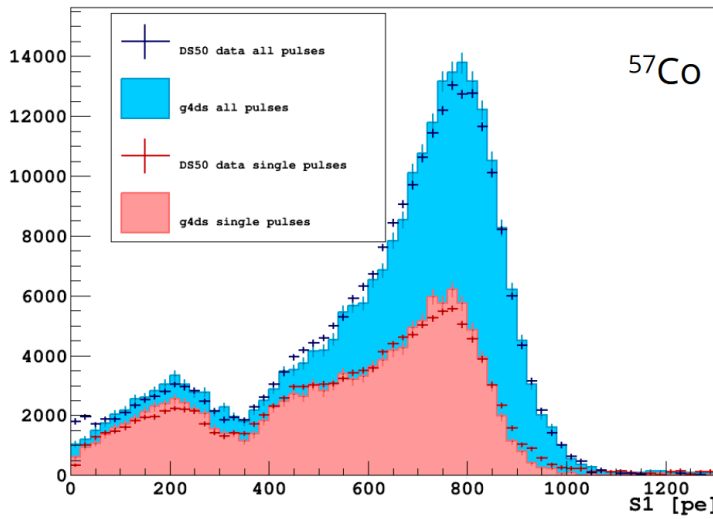
Figure 12: In black the stability of the LSV LY is monitored using internal ^{60}Co emitted from the cryostat steel, in blue the stability of the rate of radioactivity in the LSV is shown. Before and after calibration campaigns both the LY and the rate remain unaffected.

430 4.3. TPC Calibration

431 A few calibration results are shown have been collected from DarkSide
 432 papers to illustrate the quality of the acquired calibration data.

433 4.3.1. ^{57}Co S1 energy

434 Fig. 13 shows a data-MC comparison of the scintillation signal S1 spec-
 435 trum of a ^{57}Co calibration source deployed next to the cryostat and close
 436 to the TPC active volume center. Overlayed is the S1 distribution from an
 437 equivalent selection of G4DS MC simulation [?].



The plot is
from Paolo's
G4DS talk
DS2016,
UCLA.
Ideally one
could get an
official copy
from the MC
paper.

Figure 13: Data-MC comparison for the ^{57}Co source deployed next to the cryostat. In the magenta distribution a single-site interaction requirement has been imposed as for dark matter events and for the blue distribution this constraint has been removed [?].

438 4.3.2. F90 distribution from $^{241}\text{Am}^9\text{Be}$ neutron data

439 Fig. 14 shows good agreement between F90 medians and S1 spectra
 440 measured from $^{241}\text{Am}^9\text{Be}$ neutron data and those derived from SCENE
 441 measurements, which have been used to determine the nuclear recoil en-
 442 ergy scale and NR acceptance regions for the WIMP dark matter search
 443 [? 54].

444 4.3.3. Source position

445 Tests at LNGS established the deployment system's positioning ac-
 446 curacy to be about ± 1 cm after a 7 meter journey into the DarkSide-50

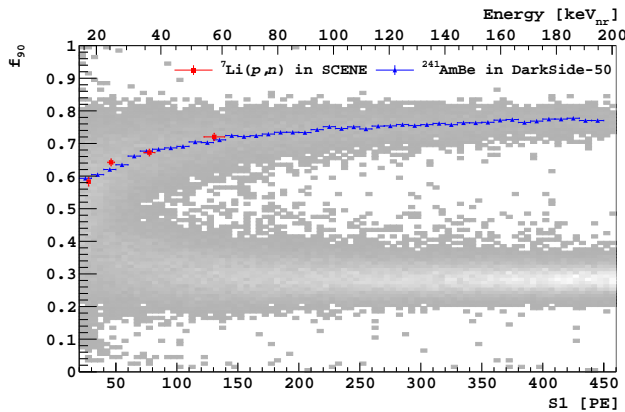


Figure 14: Plot of f_{90} vs. scintillation signal S_1 from a high rate AmBe neutron source calibration of DarkSide-50 in grey, the upper NR band from the AmBe calibration and lower ER band from β - γ backgrounds are visible. Overlayed are f_{90} NR median vs. S_1 from a high-rate *in situ* AmBe calibration (blue) and scaled from SCENE measurements (red points) [26]. There is very good agreement between the two. The high source intensity and correlated neutrons and γ -ray emission by the AmBe source contribute events outside the nuclear recoil and electron recoil bands. (reproduced from [54])

447 detector. During the first calibration campaign several runs have been
 448 taken with the source at its central position (731000 motor step counts).
 449 Fitting the t_{drift} distribution at that position a systematic shift vs. time
 450 has been observed (Fig. 15, right). Overall on average the source posi-
 451 tion has been positioned 157.4 mm below the grid with an RMS of 10.1
 452 mm. Following that observed shift the deployment procedures have been
 453 revised to avoid such a time dependency in the future and to improve
 454 the deployment precision. It is worth mentioning though that this does
 455 not induce significant uncertainties for dark matter searches, as the t_{drift}
 456 distribution can be measured *in-situ* on a per-run basis.

457 For the XY position the distribution of the azimuthal angle in the XY
 458 plane has been studied and a mean of 139 degrees has been observed
 459 with an RMS of 1.2 deg. (One degree corresponds to 6 mm at the outer
 460 cryostat, where the source is positioned.) However an independent XY
 461 reconstruction algorithm gave 142.5 degrees with an RMS of 0.8 deg, so
 462 that systematic uncertainties dominate over the XY precision [?].

463 4.4. Liquid Scintillator Veto

464 In Fig. 16, left a data-MC comparison of the LSV charge spectra from
 465 the ^{137}Cs source deployed in the LSV next to the cryostat is shown [?].

This is from
DocDB
1288. Ideally
one could cite
a XY paper
here, which is
not published
yet.

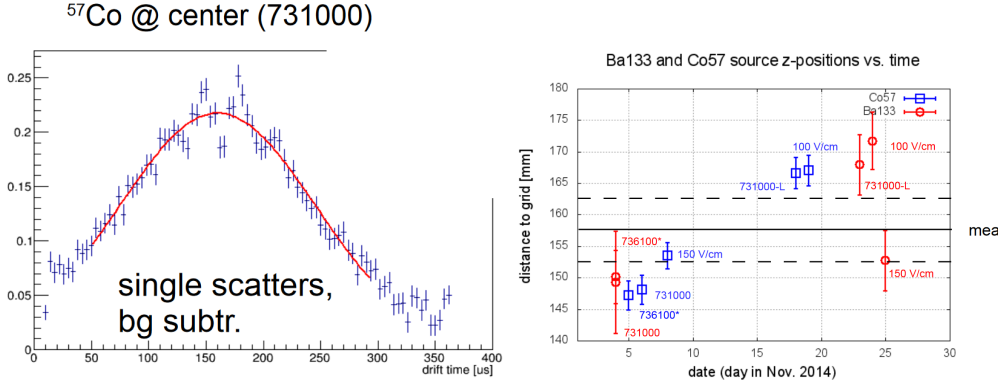


Figure 15: *left*: A t_{drift} distribution encoding the z-position of the ^{57}Co deployed next to the TPC center. *right*: Shift of source position relative to the TPC grid as a function of time when deployed to the same place.

466 In January and February 2015 the reconstitution of the LSV scintillator
 467 was completed and a second AmBe neutron source calibration of the LSV
 468 calibration was undertaken to further study the various neutron detection
 469 channels in the LSV. With a borated scintillator, a critical aspect of the
 470 neutron detection efficiency is the capability to observe the 6.4 % capture
 471 branch leading to a 1775 keV $\alpha + ^7\text{Li}(\text{g.s.})$ without the accompanying 478
 472 keV γ -ray. As shown in Fig. 16, right the de-excitation channel is clearly
 473 observed at around 30 PE.

474 5. Conclusions

475 summarize that the LSV and TPC detector have not been negatively
 476 affected.

477 Refer to the next generation DS-detector.

- 478 [1] S.M. Faber and J.S. Gallagher, *Ann. Rev. Astron. Astroph.* **17**, 135
 479 (1979).
- 480 [2] D.N. Spergel et al., *Ap. J. Supp.* **148**, 175 (2003).
- 481 [3] Committee on Elementary Particle Physics in the 21st Century of the
 482 National Academies of Science, *Revealing the Hidden Nature of Space*
 483 *and Time: Charting the Course for Elementary Particle Physics*, Page 118,
 484 National Academies Press, Washington, DC (2006).
- 485 [4] M.W. Goodman and E. Witten, *Phys. Rev. D* **31**, 3059 (1985).

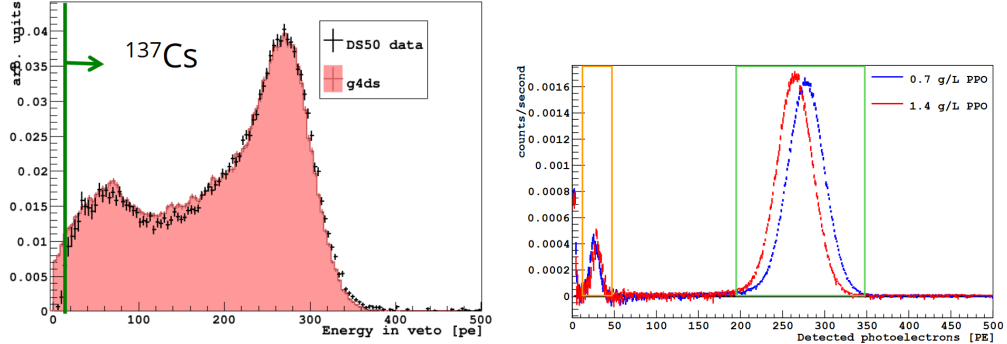


Figure 16: *left*: Data-MC comparison of the LSV charge spectra from the ^{137}Cs source deployed in the LSV next to the cryostat [?]. *right*: Clear detection of the neutron capture signal on ^{10}B in the LSV leading to a 1775 keV α + $^7\text{Li}(\text{g.s.})$ at ≈ 30 PE (orange box). The peak on the right at ≈ 270 PE (green box) is from the 93.6 % of captures that lead to the ^7Li excited state reaction, with the accompanying 478 keV-ray. The entries below 10 PE are due to PMT after-pulses. Data has been taken before and after varying the concentration of the wavelength shifter PPO in the scintillator with the source rotated 70 cm away from the cryostat. In both cases the deexcitation to ground state is clearly observed.[?]

- [5] P. Benetti et al. (WARP Collaboration), [Astropart. Phys.](#) **28**, 495 (2008).

[6] T. Alexander et al. (DarkSide Collaboration), [Astropart. Phys.](#) **49**, 44 (2013).

[7] H.O. Back et al., [arxiv:1204.6024](#).

[8] H.O. Back et al., [arxiv:1204.6061](#).

[9] H.H. Loosli, [Earth Plan. Sci. Lett.](#) **63**, 51 (1983).

[10] P. Benetti et al. (WARP Collaboration), [Nucl. Inst. Meth. A](#) **574**, 83 (2007).

[11] J. Xu et al., [Astropart. Phys.](#) **66**, 53 (2015).

[12] G. Alimonti et al. (Borexino Collaboration), [Astropart. Phys.](#) **8**, 141 (1998).

[13] G. Alimonti et al. (Borexino Collaboration), [Nucl. Instr. Meth. A](#) **406**, 411 (1998).

- 500 [14] G. Bellini et al. (Borexino Collaboration), *JCAP* **1308**, 049 (2013).
- 501 [15] G. Alimonti et al. (Borexino Collaboration), *Nucl. Instr. Meth. A* **600**,
502 **568** (2009).
- 503 [16] G. Alimonti et al. (Borexino Collaboration), *Nucl. Instr. Meth. A* **609**,
504 **58** (2009).
- 505 [17] M. G. Boulay and A. Hime, *Astropart. Phys.* **25**, 179 (2006).
- 506 [18] G. Bellini et al. (Borexino Collaboration), *Phys. Rev. Lett.* **107**, 141302
507 (2011).
- 508 [19] G. Bellini et al. (Borexino Collaboration), *Phys. Rev. D* **89**, 112007
509 (2014).
- 510 [20] F.P. An et al. (Daya Bay Collaboration), [arxiv:1407.0275](https://arxiv.org/abs/1407.0275).
- 511 [21] http://www.toray.jp/films/en/properties/lumirror/lum_e6sr.html, archived at https://web.archive.org/web/20110405061457/http://www.toray.jp/films/en/properties/lumirror/lum_e6sr.html.
- 515 [22] A. Wright, P. Mosteiro, and F. Calaprice, *Nucl. Instr. Meth. A* **644**, 18
516 (2011).
- 517 [23] L.R. Greenwood and N.R. Chellew, *Rev. Sci. Instr.* **50**, 466 (1979).
- 518 [24] S.C. Wang et al., *Nucl. Instr. Meth. A* **432**, 111 (1999).
- 519 [25] T. Alexander et al. (SCENE Collaboration), *Phys. Rev. D* **88**, 092006
520 (2013).
- 521 [26] T. Alexander et al. (SCENE Collaboration), [arxiv:1406.4825](https://arxiv.org/abs/1406.4825).
- 522 [27] www.saesgetters.com, archived at <https://web.archive.org/web/20141222175229/http://www.saesgetters.com/>.
- 524 [28] D. Vénos, A. Špalek, O. Lebeda, M. Fišer, *Appl. Rad. Isotopes* **63**, 323
525 (2005).
- 526 [29] W.H. Lippincott, S.B. Cahn, D. Gastler, L.W. Kastens, E. Kearns,
527 D.N. McKinsey, and J.A. Nikkel, *Phys. Rev. C* **81**, 045803 (2010).

- 528 [30] S. Kubota, M. Hishida, and A. Nohara, *Nucl. Instr. Meth.* **150**, 561,
529 (1978); M.J. Carvalho and G. Klein, *J. Lumin.* **18-19**, 487 (1979);
530 J.W. Keto, R.E. Gleason, and F.K. Soley, *J. Chem. Phys.* **71**, 2676
531 (1979); T. Suemoto and H. Kanzaki, *J. Phys. Soc. Japan* **46**, 1554
532 (1979); S. Kubota, M. Hishida, M. Suzuki, J-z. Ruan, *Nucl. Instr.*
533 *Meth.* **196**, 101 (1982); S. Kubota et al., *Phys. Rev. B* **20**, 3486 (1979).
- 534 [31] A. Hitachi, T. Takahashi, N. Funayama, K. Masuda, J. Kikuchi, and
535 T. Doke, *Phys. Rev. B* **27**, 5279 (1983).
- 536 [32] E. Shibamura, K. Masuda, and T. Doke, Research Report to the Min-
537 istry of Education, Science, Sport, and Culture for Grant-in-Aid Sci-
538 entific Research(C), No. 62540284 (1988).
- 539 [33] P. Benetti et al., *Nucl. Instr. Meth. A* **327**, 203 (1993).
- 540 [34] P. Agnes et al. (DarkSide Collaboration), [arxiv:1412.2969](https://arxiv.org/abs/1412.2969).
- 541 [35] www.caen.it, archived at
542 <https://web.archive.org/web/20150104083159/http://www.caen.it/>.
- 543 [36] www.ni.com, archived at
544 <https://web.archive.org/web/20150218101935/http://www.ni.com/>.
- 545 [37] www.highlandtechnology.com, archived at <https://web.archive.org/web/20150215110202/http://www.highlandtechnology.com/>.
- 546 [38] C. Green et al., *J. Phys. Conf. Ser.* **396**, 022020 (2012).
- 547 [39] A. Empl, R. Jasim, E.V. Hungerford, and P. Mosteiro, *JCAP* **1408**, 64
548 (2014).
- 549 [40] T. Pollmann, M. Boulay, and M. Kuzniak, *Nucl. Instrum. Meth. A*
550 **635**, 127 (2011).
- 551 [41] A. Pocar, *Low Background Techniques and Experimental Challenges for*
552 *Borexino and its Nylon Vessels*, Ph.D. Dissertation, Princeton Univer-
553 sity (2003). search.proquest.com/docview/288218433/abstract.
- 554 [42] J. Benziger et al., *Nucl. Instr. Meth. A* **582**, 509 (2007).

- 558 [43] B. Aharmim et al. (SNO Collaboration), *Phys. Rev. Lett.* **101**, 111301
559 (2008).
- 560 [44] W.H. Lippincott, K. J. Coakley, D. Gastler, A. Hime, E. Kearns,
561 D.N. McKinsey, J.A. Nikkel, and L.C. Stonehill, *Phys. Rev. C* **78**,
562 035801 (2008). Note that there is a misprint in the relevant equation
563 11.
- 564 [45] M.G. Boulay et al. (DEAP Collaboration), [arxiv:0904.2930](#).
- 565 [46] J.D. Lewin and P. Smith, *Astropart. Phys.* **6**, 87 (1996).
- 566 [47] C. Savage, K. Freese, and P. Gondolo, *Phys. Rev. D* **74**, 043531 (2006).
- 567 [48] M.C. Smith et al., *Mon. Not. Roy. Astron. Soc.* **379**, 755 (2007).
- 568 [49] C. Savage, G. Gelmini, P. Gondolo, and K. Freese, *JCAP* **0904**, 010
569 (2009).
- 570 [50] D.S. Akerib et al. (LUX Collaboration), *Phys. Rev. Lett.* **112**, 091303
571 (2014).
- 572 [51] E. Aprile et al. (XENON100 Collaboration), *Phys. Rev. Lett.* **109**,
573 181301 (2012).
- 574 [52] M. Xiao et al. (PandaX Collaboration), [arxiv:1408.5114](#).
- 575 [53] Z. Ahmed et al. (CDMS II Collaboration), *Science* **327**, 1619 (2010).
- 576 [54] P. Agnes et al. (DarkSide Collaboration), Results from the first use
577 of low radioactivity argon in a dark matter search, *Phys. Rev. D* **93**,
578 081101 (2016) [arxiv:1510.00702](#)